Journal of Materials Chemistry

Cite this: *J. Mater. Chem.*, 2012, **22**, 21998

www.rsc.org/materials

PAPER

The GO/rGO–Fe_3O_4 composites with good water-dispersibility and fast magnetic response for effective immobilization and enrichment of biomolecules†

Gong Cheng,[abd] Yan-Lin Liu,[bd] Zhi-Gang Wang,[bd] Ji-Lin Zhang,*[b] De-Hui Sun[c] and Jia-Zuan Ni*[ab]

Received 8th June 2012, Accepted 24th August 2012
DOI: 10.1039/c2jm33695b

The graphene oxide (GO)–Fe_3O_4 and the reduced graphene oxide (rGO)–Fe_3O_4 composites with good water dispersibility, high affinity and rapid magnetic response have been prepared *via* a facile grafting method. They can be used for the effective immobilization of proteins and the enrichment of peptides, respectively. By taking advantage of the high loading capacity and the abundant hydrophilic groups of the GO–Fe_3O_4 composites, they can be applied to immobilize proteins. The amount of loading of protein (BSA) on GO–Fe_3O_4 is as high as 294.54 mg g^{-1}. The rGO–Fe_3O_4 composites can be used to enrich the low-concentration peptides conveniently due to their high surface areas, special structures and strong magnetism. Nineteen target peptides with the sequence coverage of 21% can be enriched and detected from the highly diluted digest of BSA (5 fmol μL^{-1}). These results reveal that the prepared GO/rGO–Fe_3O_4 composites have potential application as a carrier for biomolecule immobilization, enrichment, and separation.

Introduction

As a new class of two-dimensional carbon nanostructure, graphene has received increasing attention in various fields due to its attractive electronic, catalytic, mechanical, optical, and magnetic properties as well as available hydrophobicity.[1–5] Notably, the large delocalized π-electron system and ultrahigh specific surface area of graphene endow it with a strong affinity and high loading capacity for hydrophobic biomolecules and carbon-based ring structures.[6–9] Graphene oxide (GO), the oxidized derivative of graphene, is highly hydrophilic and water soluble because it possesses various functional groups such as epoxide, carboxyl, and hydroxyl. They can also undergo covalent, electrostatic, or hydrogen bonding for functional modification, which makes them more suitable for bio-application.

Recently, graphene and graphene oxide were developed as fascinating and promising candidate materials in biomedical applications such as drug delivery carriers of high efficiency, purification and detection of biomolecules, immobilization of enzymes, and enrichment of proteins.[10–13] For example, Tang and co-workers[14] demonstrated that graphene can be used as an ultrahigh efficiency preconcentration and detection platform for DNA oligomers for direct mass spectrometry (MS) analysis. Furthermore, the aptamer-conjugated graphene oxide composites were prepared and used as an affinity extraction and detection platform for analytes from complex biological media.[15] Despite these developing achievements, the direct use of graphene or graphene oxide as adsorbents for bio-application has several disadvantages. First, it is difficult to collect the small graphene or graphene oxide sheets from a well-dispersed solution *via* filtration and centrifugation. Second, the direct separation of graphene or graphene oxide sheets easily results in the irreversible aggregation of them, which may reduce the adsorption capacity and the adsorption efficiency. Therefore, optimizing the surface properties of the graphene or graphene oxide sheets by further functionalization for convenient separation and high adsorption efficiency is required.

As a promising separation tool in bio-application, the Fe_3O_4 particles-based magnetic isolation has become an effective separation technique.[16–19] Recently, some graphene–Fe_3O_4 hybrid materials have been explored for energy storage, water treatment, preconcentration of small molecules and drug delivery.[20–23] However, there still exist the following problems which are not in favor of the bio-applications: (1) poor control over the size, size distribution, and location of magnetic Fe_3O_4 nanoparticles on the graphene oxide or graphene sheets; (2) they may agglomerate and gradually precipitate from their aqueous suspension due to the poor water dispersibility of the hydrophobic graphene.[24,25] Although some polymer-additives were

[a]*Key Laboratory of Marine Bioresources and Ecology, College of Life Science, Shenzhen University, Shenzhen 518060, China*
[b]*State Key Laboratory of Rare Earth Resource Utilization, Changchun Institute of Applied Chemistry, Chinese Academy of Sciences, Changchun 130022, China. E-mail: zjl@ciac.jl.cn*
[c]*Changchun Institute Technology, Changchun 130012, China*
[d]*Graduate University of the Chinese Academy of Sciences, Beijing 100049, PR China*

† Electronic supplementary information (ESI) available. See DOI: 10.1039/c2jm33695b

used to produce water-dispersible graphene–Fe_3O_4 hybrid materials,[26,27] they could be undesirable for practical applications. Additionally, the graphene-based magnetic hybrid materials with good water dispersibility for effective protein immobilization and enrichment of low-concentration peptides as well as easy magnetic separation have not yet been reported.

In this study, the GO/rGO–Fe_3O_4 composites with good water dispersibility and fast magnetic response have been prepared *via* a facile grafting method and applied for biomolecule immobilization and enrichment. As shown in Scheme 1a, the GO was first grafted by (3-mercaptopropyl)trimethoxysilane (MPS) with mercapto group, and then the spherical Fe_3O_4 particles with different sizes were controlled to covalently attach on the GO nanosheets. The obtained product is denoted as GO–Fe_3O_4. After the reduction of GO–Fe_3O_4 in alkaline aqueous solution under mild conditions, the water-dispersible reduced graphene oxide–Fe_3O_4 composites (denoted as rGO–Fe_3O_4) were obtained. The GO/rGO–Fe_3O_4 composites with good water-dispersity and fast magnetic response combine the merits of the easy separation of Fe_3O_4 and high affinity of graphene and graphene oxide. These composites have been demonstrated to be a potential platform for protein immobilization and peptide enrichment. The prepared GO–Fe_3O_4 composites can be used as effective adsorbents for protein immobilization by virtue of their high loading capacity and the abundant hydrophilic groups, while rGO–Fe_3O_4 composites with high surface areas and hydrophobicity possess great potential for peptide enrichment.

Experimental

Materials

Graphite powder, urea, ammonium bicarbonate (NH_4HCO_3), ferric chloride hexahydrate ($FeCl_3 \cdot 6H_2O$), ethylene glycol (EG), diethylene glycol (DEG), ethylenediamine (EN) and sodium acetate (NaAc) were purchased from China National Pharmaceutical Group Corporation (Shanghai, China). (3-Mercaptopropyl)trimethoxysilane (98%, MPS), polyethylene glycol (M_w 1000, PEG), acetonitrile (ACN), 2,5-dihydroxybenzoicacid (2,5-DHB), dithiothreitol (DTT) and bovine serum albumin (98%, BSA) were purchased from Aladdin (Shanghai, China). Trypsin (from bovine pancreas, TPCK treated) was purchased from Sigma-Aldrich (St. Louis, MO, USA). Iodoacetamide (IAA) was purchased from Alfa Aesar (USA). $K_2S_2O_8$, P_2O_5, $KMnO_4$, H_2O_2 (30%), H_2SO_4, HCl and ethanol were all analytical grade reagents and were obtained from Beijing Chemical Regent Co. Ltd. (Beijing, China).

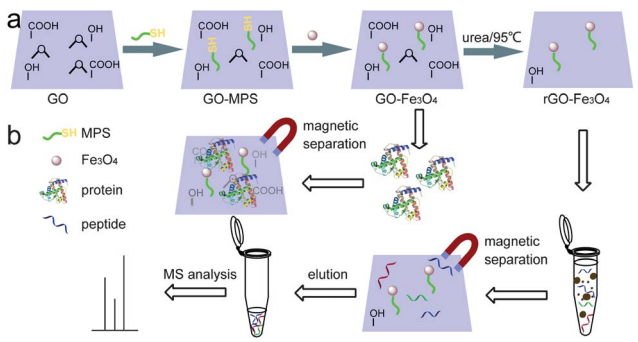

Scheme 1 Schematic illustration of the synthesis strategy of the GO–Fe_3O_4 and rGO–Fe_3O_4 composites (a), and their application in protein immobilization and peptide enrichment (b).

Preparation of GO and GO–MPS

Graphene oxide (GO) was synthesized from natural graphite powder by a modified Hummers method.[28,29] For the preparation of mercapto group-functionalized GO, 15 mg GO was dispersed into 20 mL ethanol *via* ultrasonication for 30 min. Then, the dispersion system was bubbled with nitrogen for 30 min under mechanical agitation. Subsequently, 0.25 mL MPS was slowly added into the dispersion system under nitrogen atmosphere, and then the system was mechanically stirred for 12 h at 70 °C in a water bath. The obtained GO–MPS product was separated by centrifugation, and then washed with ethanol three times to remove the unreacted MPS.

Preparation of superparamagnetic Fe_3O_4 particles with different sizes

For the synthesis of 60 nm Fe_3O_4 nanoparticles, $FeCl_3 \cdot 6H_2O$ (2.50 g) was injected into a mixture containing 8.9 mL EN and 80 mL EG under magnetic stirring, followed by the addition of NaAc (5.00 g). The mixture was transferred to a Teflon-lined stainless-steel autoclave and sealed, to heat at 200 °C for 6 h. The produced magnetite nanoparticles were washed with deionized water, and separated using a magnet, and finally dried in an oven at 80 °C for 12 h. Synthesis of 200 nm Fe_3O_4 nanoparticle is similar to the above synthetic process except $FeCl_3 \cdot 6H_2O$ (2.70 g), EN (10 mL) and additive PEG (2.00 g) were used. 500 nm Fe_3O_4 microspheres were prepared following a literature method reported previously.[30]

Preparation of GO–Fe_3O_4 and rGO–Fe_3O_4 composites

The GO–Fe_3O_4 composites were prepared by the following method. 15 mg of the obtained Fe_3O_4 particles were pretreated with 25 mL 0.1 M hydrochloric acid *via* ultrasonication for 30 min. Then, the particles were separated *via* a magnet and washed with deionized water and ethanol 3 times. The above particles and GO–MPS were re-dispersed into 15 mL ethanol *via* ultrasonication for 30 min. The particle suspension was added dropwise into the GO–MPS solution under agitation. The mixture was further stirred for 24 h at room temperature. Finally, the GO–Fe_3O_4 particles were collected by a magnet, and then washed with deionized water and ethanol several times.

The rGO–Fe_3O_4 composites were prepared *via* reducing the GO–Fe_3O_4 composites in alkaline aqueous solution under mild conditions.[31,32] In brief, the as-prepared GO–Fe_3O_4 composites were well-dispersed into 30 mL deionized water, and the pH value of the GO–Fe_3O_4 dispersion solution was adjusted to 8.0 using dilute ammonia solution. Subsequently, 1.0 g urea was added into the solution mixture under agitation, and then the solution mixture was heated to 95 °C. After stirring for 48 h, the rGO–Fe_3O_4 composites were collected by magnetic separation, and washed with deionized water several times.

Tryptic digest of proteins

1 mg protein (BSA) was dissolved in 0.5 mL 50 mM NH_4HCO_3 solution containing urea (4.0 mmol, 8 M). 50 μL 100 mM DTT solution was added into the protein solution, and then the system was maintained at 60 °C for 1 h. After that, 50 μL of 200 mM IAA solution was added into the above solution, followed by shaking for 2.5 h at room temperature. After denaturation by the above step, trypsin was added into the solution with a molar ratio of 50 : 1 (BSA : trypsin), and the solution was incubated at 18 h at 37 °C. Finally, the obtained tryptic digests were diluted to the target concentration.

Adsorption of biomolecules by GO–Fe_3O_4 composites

The GO–Fe_3O_4 composites (2 mg mL^{-1}) were dispersed into a phosphate buffer (PBS) prior to adsorption. 0.5 mL of the GO–Fe_3O_4 suspended solution (2 mg mL^{-1}) was mixed with 0.5 mL of the BSA solution in PBS with designed concentrations, followed by shaking for three hours so as to ensure reaching equilibration. The supernatant was collected after magnetic separation. The adsorption curves were obtained by measuring the solution absorbence at 280 nm before and after the treatment using UV-vis spectroscopy and a calibration curve. The amount of the adsorbed biomolecules was calculated using the following equation:

$$Q_e = \frac{(C_0 - C_e)V}{m} \quad (1)$$

where Q_e is the concentration of the adsorbed biomolecules (mg g^{-1}), C_0 and C_e are the initial and the equilibrium concentrations of protein, respectively. V is the volume of the solution, and m is the weight of the added GO–Fe_3O_4 composites.

Enrichment of low-abundance peptides

1000 μL (5 fmol μL^{-1}) BSA digest was mixed with 10 μL of 35 mg mL^{-1} Fe_3O_4 or rGO–Fe_3O_4 composites suspended solution and then shaken for 15 min. Subsequently, the composites trapped target peptides were collected by magnetic separation. Then, the enriched peptides were eluted with 5 μL of elution solution containing 60% ACN and 1.0% TFA, and the supernatant was collected by magnetic separation. The above products obtained from the elution step were dissolved in 50% (v/v) aqueous acetonitrile solution (2 μL) containing DHB (20 mg mL^{-1}) and H_3PO_4 (1%, v/v) by pipetting, and the mixture was then deposited onto the MALDI target for MS detection. The enrichment of peptides using the commercial Zip-TipC18 pipette tip was carried out according to the standard procedure provided by the technical note of MILLIPORE Corporation (http://www.millipore.com/techpublications/tech1/tn072).

Materials characterization

Scanning electron microscopy (SEM) images were obtained on a field emission scanning electron microscope (FESEM, S4800, Hitachi) equipped with an energy-dispersive X-ray spectrometer (EDX, JEOLJXA-840). Transmission electron microscopy (TEM) and high-resolution TEM (HRTEM) images were taken with a FEI Tecnai G2 S-Twin transmission electron microscope operated at 200 kV. Powder X-ray diffraction (XRD) patterns were collected on a Bruker D8FOCUS X-ray diffractometer using Cu Kα radiation ($\lambda = 1.5406$ Å) at a scanning rate of 15° min^{-1} and a detection range from 5° to 80°. Fourier-transform infrared spectroscopy (FTIR) analyses were carried out on a Bruker Vertex 70 FTIR Spectrometer. Magnetization measurements were carried out with a superconducting quantum interface device (SQUID) magnetometer (Quantum Design MPMS XL) at 300 K. UV/visible absorption spectra and the adsorption curves were obtained using a Shimadzu UV-1750 UV/visible spectrophotometer.

MS analysis was carried out on a Bruker Autoflex III MALDI-TOF MS (Bruker Daltonics Bremen, Germany) equipped with a 355 nm Nd-YAG laser. The acceleration voltage and repetition rate were set at 19 kV and 200 Hz, respectively, whilst the laser power was optimized until the best-quality spectrum was obtained. For peptide mass fingerprinting (PMF) data, 600 laser shots were accumulated for each spectrum, which was obtained in positive ion reflection mode and analyzed by Bruker Daltonics flex Analysis software. Search parameters: fragment ion spectra were submitted to MASCOT (http://www.matrixscience.com/) for database search and identification of corresponding peptides employing the following search parameter settings. Database: SwissProt; enzyme: trypsin; maximum of missed cleavages: 1; taxonomy: mammalia (mammals); peptide tolerance: 1.2 Da; mass values: monoisotopic.

Results and discussion

As illustrated in Scheme 1, the synthetic strategy of GO–Fe_3O_4 mainly includes functionalizing the as-synthesized GO with MPS to form GO–MPS, grafting Fe_3O_4 particles onto the GO–MPS *via* a covalent linker to produce GO–Fe_3O_4, and reducing the GO–Fe_3O_4 to rGO–Fe_3O_4 in alkaline aqueous solution with urea as the pH adjustor. The MPS is a good linking reagent with bifunctional reactive groups. Its trimethoxysilane head group can be chemically bound to GO *via* hydroxyl and epoxy groups on it, whereas the mercapto group in the tail is able to form strong covalent bonds with Fe atoms of the Fe_3O_4. Therefore, the Fe_3O_4 particles with different sizes and morphology can be easily covalently grafted onto the functional GO under mild reaction conditions.

The morphologies and structures of the as-prepared GO and the GO–Fe_3O_4 composites were characterized using scanning electron microscopy (SEM) and transmission electron microscopy (TEM). Fig. 1 gives the representative SEM and TEM images of the GO (SEM: Fig. 1a; TEM: Fig. 1b), and the GO–Fe_3O_4 composites (SEM: Fig. 1c and d; TEM: Fig. 1e–g). Compared with bare GO sheets (Fig. 1a and b), there are many Fe_3O_4 particles attached on the surfaces of the treated GO sheets (Fig. 1c and d). The Fe_3O_4 particles were well distributed on the GO sheets with nearly flat and several square micrometer area. Furthermore, no free or independent nanoparticles outside the GO sheets were observed, which indicates that all of the nanoparticles were attached to the GO. It can be distinctly observed from SEM images (Fig. 1d and S2†) that the Fe_3O_4 particles of different sizes were immobilized on both sides of the GO, which will result in a better magnetic response. TEM images and EDX detection further provide the evidences of their assembly

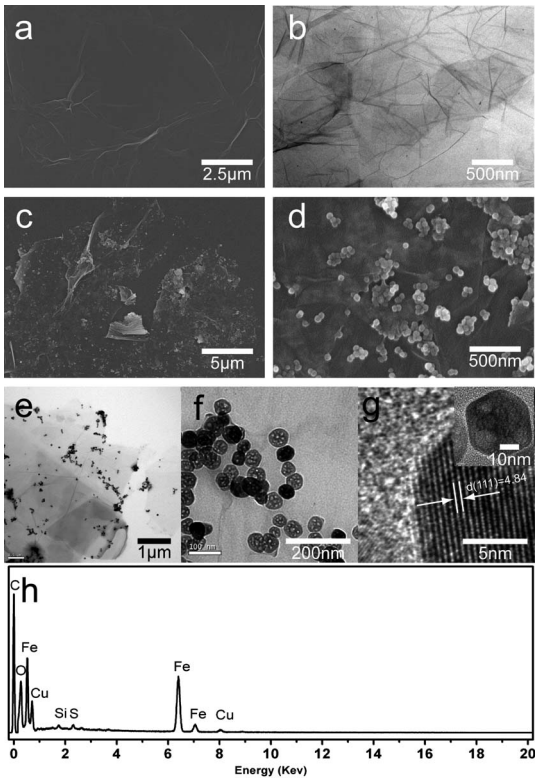

Fig. 1 SEM and TEM images of the GO (a and b) and the GO–Fe_3O_4 (c–g), and EDX spectrum of the GO–Fe_3O_4 (h).

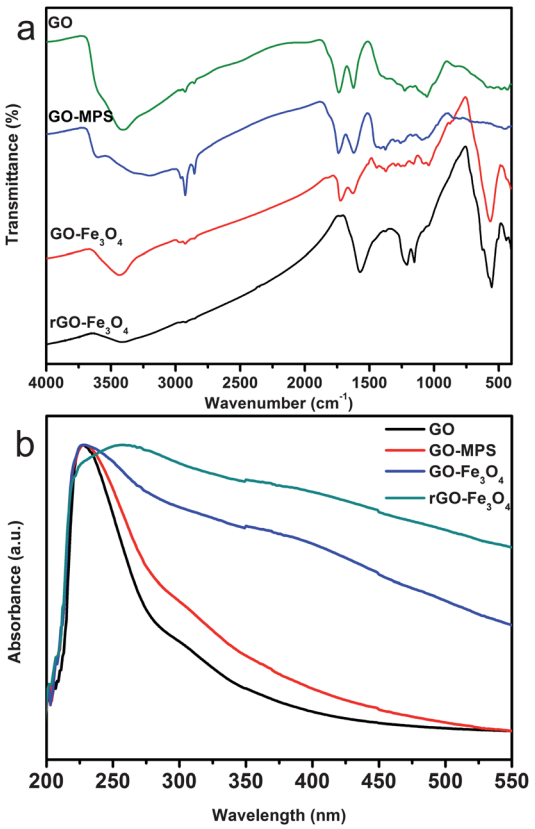

Fig. 2 FTIR spectra (a) and UV-vis spectra (b) of GO, GO–MPS, GO–Fe_3O_4 and rGO–Fe_3O_4.

(Fig. 1e–h). The average diameter of the attached Fe_3O_4 nanoparticles is about 60 nm, as shown in Fig. 1f. According to the HRTEM image (Fig. 1g), the lattice fringe spacing (0.48 nm) agrees well with the lattice spacing of (111) planes of cubic magnetite. The EDX spectrum shown in Fig. 1h indicates that the GO–Fe_3O_4 composites contain C, Fe, O, Si and S elements, while the Cu element arises from the sample carrier. It can be confirmed from these above results that even distribution of the Fe_3O_4 nanoparticles on the whole GO nanosheets can be attributed to uniform distribution of the covalent bonding sites of –SH groups.

The grafting process can be verified by FTIR and UV-vis spectra. As shown by the FTIR in Fig. 2a, the presence of O–H ($\upsilon_{(O-H)}$ at 3412 cm^{-1}), C=O ($\upsilon_{(C=O)}$ at 1733 cm^{-1} in carbonyl groups), C=C ($\upsilon_{(C=C)}$ at 1621 cm^{-1}), and C–O ($\upsilon_{(C-OH)}$ at 1226 cm^{-1} and $\delta_{(O-H)}$ at 1055 cm^{-1}) indicates the successful preparation of GO, which is in accordance with previously reported results.[1] After modification with MPS, the greatly increased intensity of the peaks at 2925 and 2854 cm^{-1} ($\upsilon_{(C-H)}$ of $-CH_3$ and $-CH_2$), the decreased intensity of the peaks at 3409 cm^{-1} ($\upsilon_{(O-H)}$) and 1055 cm^{-1} ($\upsilon_{(C-O)}$ of C–O–C), and the presence of new peaks at 1093 cm^{-1} ($\upsilon_{(Si-O)}$ of Si–O–C) and 1377 cm^{-1} ($\delta_{(C-H)}$ of S–CH_2) confirm that MPS was covalently grafted on the GO. After immobilization of Fe_3O_4 particles, a new characteristic peak (565 cm^{-1}) was observed, corresponding to the stretching vibration of the Fe–O bond. As expected, the characteristic peaks of hydrophilic groups (*e.g.* –COOH and –OH) can still be observed with high intensity, indicating the whole modification process did not lead to the reduction of the GO. Moreover, there exist more hydroxyl groups rooted in Fe_3O_4. Comparing with the spectrum of GO–Fe_3O_4, the disappearance of the peak at 1733 cm^{-1} ($\upsilon_{(C=O)}$ in carbonyl groups) in the rGO–Fe_3O_4 FTIR provides obvious evidence of the deoxygenation of GO in alkaline solution, indicating the formation of rGO–Fe_3O_4 composites, while the peaks at 1209 cm^{-1} and 1153 cm^{-1} should be ascribed to the formation of Si–O–Si bonds resulting from the further hydrolysis of partially reacted silane molecules in alkaline aqueous solution at 95 °C during the process of GO reduction.

The above conclusion can be further affirmed by the UV-vis absorption spectra (Fig. 2b). The characteristic peak at around 227 nm arising from the conjugated system of GO can be apparently observed in all the products. As expected, only slight peak shifting occurs after the covalent grafting of MPS and the immobilization of Fe_3O_4 on the GO, indicating these modifications did not result in the unique GO structure being destroyed. However, after reduction, the rGO–Fe_3O_4 absorption peak red shifted to 256 nm because the loss of the most hydrophilic groups would enhance the electronic conjugation of graphene.[33–35]

The immobilization of the Fe_3O_4 particles on GO can be further confirmed by XRD analysis. Fig. 3 shows the XRD patterns of Fe_3O_4, GO, GO–MPS, GO–Fe_3O_4 and rGO–Fe_3O_4 composites. The GO shows a very sharp diffraction peak at 10.3° corresponding to the (002) reflection of the GO. Compared with that of the GO, a broader and slightly red shifted diffraction peak is observed in the GO–MPS sample. The modification of the MPS could result in a subtle difference in the horizontal

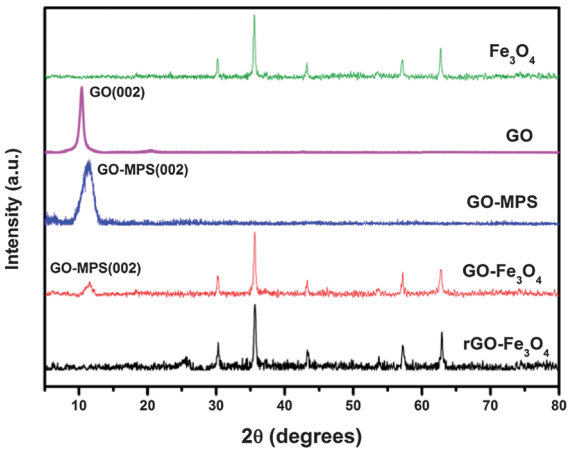

Fig. 3 XRD patterns of Fe_3O_4, GO, GO–MPS, GO–Fe_3O_4 and rGO–Fe_3O_4.

offset between layers in the GO–MPS.[36,37] After attachment of Fe_3O_4 particles, some additional diffraction peaks appeared. They can be assigned to the characteristic diffraction peaks from Fe_3O_4 (JCPDS card no. 65-3107), which is consistent with the precursor Fe_3O_4 particles. The above results demonstrate that structures of the Fe_3O_4 particles and the GO are almost unchanged after the mild modification. However, a visible shift of the (002) reflection peak from 10.3 to 25.3° on the rGO–Fe_3O_4 XRD is observed, indicating the decrease of the interlayer space due to removing of the interbedded oxygen.[37,38]

Their magnetic property provides a rapid and convenient means for the separation of GO–Fe_3O_4 and rGO–Fe_3O_4 composites, being free of the repeated centrifugation for practical applications. The magnetic properties of the Fe_3O_4 and GO–Fe_3O_4 and rGO–Fe_3O_4 were examined at 300 K *via* a superconducting quantum interface device (SQUID) magnetometer. As revealed in the hysteresis loops (Fig. 4), both the GO–Fe_3O_4 and rGO–Fe_3O_4 composites show a strong superparamagnetism at room temperature. The saturation magnetization values of Fe_3O_4, GO–Fe_3O_4 and rGO–Fe_3O_4 composites are 77.6, 33.0 and 36.9 emu g^{-1}, respectively. Though the saturation magnetizations of GO–Fe_3O_4 and rGO–Fe_3O_4 composites are less than that of the precursor magnetite particles, they are strong enough for effective magnetic separation.

The water-dispersibility of the GO/rGO–Fe_3O_4 composites was investigated by dispersing them into water. For comparison, the Fe_3O_4 particles and the graphene–Fe_3O_4 composites prepared *via* the conventional solvothermal route (denoted as G–Fe_3O_4) were also investigated. As shown in Fig. S3,† an obvious aggregation and precipitation quickly occurred in the suspension of the graphene–Fe_3O_4 composites prepared *via* the reported solvothermal method.[38] However, the GO/rGO–Fe_3O_4 suspensions were almost unchanged, indicating they are much more stable than the former. Furthermore, a comparison experiment was carried out to prove that the covalent conjugation is superior to the electrostatic attachment between Fe_3O_4 and the GO or rGO. The GO/Fe_3O_4 electrostatic attachment composite was first prepared by directly mixing the Fe_3O_4 particles and the GO without modification with MPS under the same conditions as the GO–Fe_3O_4. Then the rGO/Fe_3O_4 electrostatically attached composite was obtained *via* the same reduction process as the rGO–Fe_3O_4. Subsequently, the GO/Fe_3O_4, rGO/Fe_3O_4, GO–Fe_3O_4 and rGO–Fe_3O_4 were respectively dispersed into water by agitation on a shaker for 30 min. Then, these suspensions were attracted using the same magnet for 10 min. The experimental results indicate that, for the GO/Fe_3O_4 and the rGO/Fe_3O_4 systems, as revealed in Fig. 5a and b, although the Fe_3O_4 particles attached to the GO or rGO can be attracted to one side of the vial near the magnet, the separated solution is still opaque due to the existence of suspended GO or rGO sheets. By contrast, the GO–Fe_3O_4 and the rGO–Fe_3O_4 composites can be easily separated by the external magnet (see Fig. 5c and d), indicating that the GO–Fe_3O_4 and the rGO–Fe_3O_4 composites with good water dispersibility and excellent magnetic response are in favour of absorption and convenient separation of biomolecules. Moreover, the dispersed systems with good water dispersibility are stable enough to meet our testing requirement.

Affinity immobilization and separation of proteins and peptides have aroused great interest in the past two decades, which are widely applied in biosensors, biocatalysis, and purification of biosamples.[39–41] Since GO with many hydrophilic functional groups can incorporate biomolecules by covalent, electrostatic or hydrogen bonding interactions,[42,43] the GO–Fe_3O_4 magnetic composites can be applied to immobilize and magnetically separate proteins from solution. As an example, the

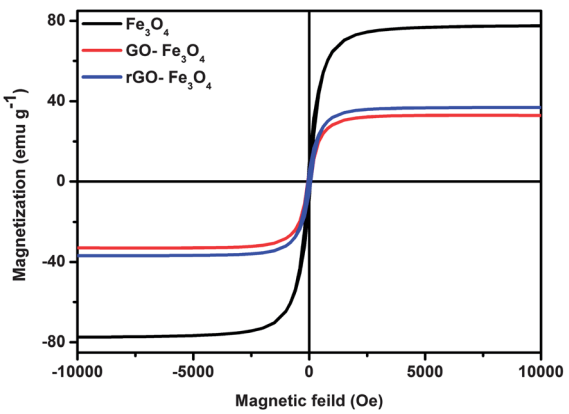

Fig. 4 Room-temperature hysteresis loops of Fe_3O_4, GO–Fe_3O_4 and rGO–Fe_3O_4.

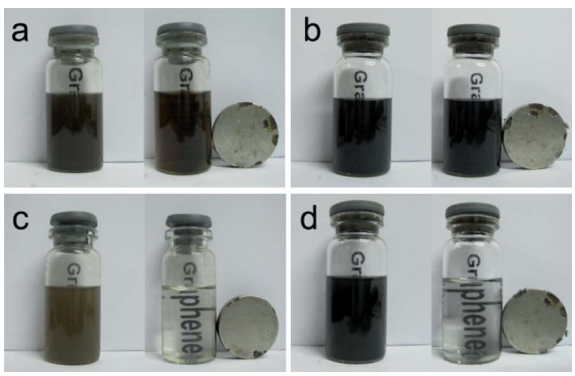

Fig. 5 Magnetic response photos of the GO/Fe_3O_4 (a), the rGO/Fe_3O_4 (b), the GO–Fe_3O_4 (c) and the rGO–Fe_3O_4 (d) aqueous solution systems.

GO–Fe_3O_4 (60 nm) composites have been investigated. Bovine serum albumin (BSA), a very abundant protein in bovine blood, was chosen as a model protein to evaluate the ability of GO–Fe_3O_4 composites for protein immobilization. The amount of Fe_3O_4 particles attached on the surface of GO is a critical factor in determining the adsorption of proteins. A higher loading of Fe_3O_4 will enhance the magnetic properties of GO–Fe_3O_4,[44] while it will decrease the exposed surface area of GO simultaneously, thus resulting in a lower adsorption capacity. Therefore, three ratios of GO to Fe_3O_4 composites have been prepared for investigating the protein immobilization. As shown in Fig. S4,† the adsorption ability increase with the ratio of GO to Fe_3O_4. However, it is hard to magnetically separate the GO–Fe_3O_4 composites rapidly when the ratio of GO to Fe_3O_4 is as high as 2 : 1, due to the low Fe_3O_4 content in the composites. When the ratio of Fe_3O_4 to GO is 1 : 1, a relatively optimal result can be obtained. Therefore, we chose GO–Fe_3O_4 composites with the ratio of Fe_3O_4 to GO (1 : 1) as models to further investigate their applications. Meanwhile, adsorption abilities of Fe_3O_4, GO–Fe_3O_4 and rGO–Fe_3O_4 were compared using BSA solution (1 mg mL^{-1}). Apparently, the composites show much better adsorption abilities than the bare Fe_3O_4 particles, and the GO–Fe_3O_4 composites show the best adsorption ability (Fig. S5†). This can be attributed to the high surface area and the hydrophilic functional groups on the surface of GO in the GO–Fe_3O_4 composites.

Fig. 6 shows the UV-vis absorption spectra of the BSA solution with initial concentration of 0.125 mg mL^{-1} before and after adsorption by the GO–Fe_3O_4 composites. The wavelength with maximum absorbance (280 nm) was used as detecting wavelength. For 0.125 mg mL^{-1} of the BSA solution, 51.65% of the BSA can be removed or immobilized. The adsorption capacity can be judged from the absorption curve (inset). Obviously, the adsorbed amount of the BSA gradually increased with the increase of the equilibrium concentration. When the concentration of BSA is 2.0 mg mL^{-1}, the adsorption capacity of the proteins adsorbed by GO–Fe_3O_4 composites is 294.54 mg g^{-1}. The high adsorption capacity stems from strong interactions between the BSA protein and the oxygen-containing functional groups on the GO–Fe_3O_4 composites.

In proteomics, many low-abundance endogenous peptides can be used as biomarkers with high clinical sensitivity and specificity, which could provide valuable information for the detection of many diseases and elucidation of pathological variations.[45] However, it is a great challenge to detect the low-abundance peptides directly due to their extremely low concentrations and the interference of salts. Graphene has a great potential for adsorption of biomolecules due to its high specific surface area, hydrophobicity and unique conjugation structure. Thus, the rGO–Fe_3O_4 composites can be applied as an affinity probe for enrichment of low-abundance peptides by taking advantage of the special properties of rGO and the rapid magnetic response of Fe_3O_4. As an example, the tryptic digests of BSA are employed to demonstrate the possibility for enrichment and rapid separation of low-abundance peptides. Fig. 7 shows the MALDI-TOF mass spectra of the diluted tryptic digest of BSA before and after treatment with the rGO–Fe_3O_4 composites. Apparently, only three peptides (marked with '*') with the low signal-to-noise (*S*/*N*) ratio can be detected from the diluted BSA digest (Fig. 7a) due to the low concentration of target peptides and the interference of salts used in the digestion process. However, after enrichment with the rGO–Fe_3O_4 composites, nineteen peptides with the sequence coverage of 21% (Table S1†) could be assigned to BSA with increased *S*/*N* ratio and intensity, indicating the rGO–Fe_3O_4 composites can enrich the low-abundance peptides (Fig. 7b). For comparison, the pure Fe_3O_4 particles are used to enrich the peptides. After treatment using the Fe_3O_4 particles, nine peptides can be observed with slightly increased *S*/*N* ratio, while most of the peptides with low molecular weight are lost (Fig. S7a†). In addition, a commercial Zip-TipC18 pipette tip is also used to enrich the peptides. Apparently, only a few peptides with lower *S*/*N* ratio can be observed (Fig. S7b†) after the solution was treated by a Zip-TipC18 pipette tip. The above results indicate the prepared rGO–Fe_3O_4 composites show good potential for enriching low molecular weight peptides. The hydrophobic interactions between the rGO–Fe_3O_4 composites and the exposed hydrophobic residues of the low molecular

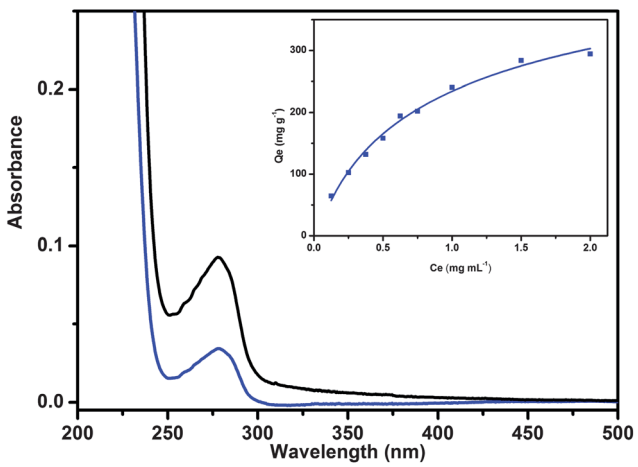

Fig. 6 UV-vis absorption spectra of 0.125 mg mL^{-1} of the BSA solution before (black) and after adsorption by the GO–Fe_3O_4 (blue) and adsorption isotherm of different concentrations of BSA onto the GO–Fe_3O_4 composite (inset).

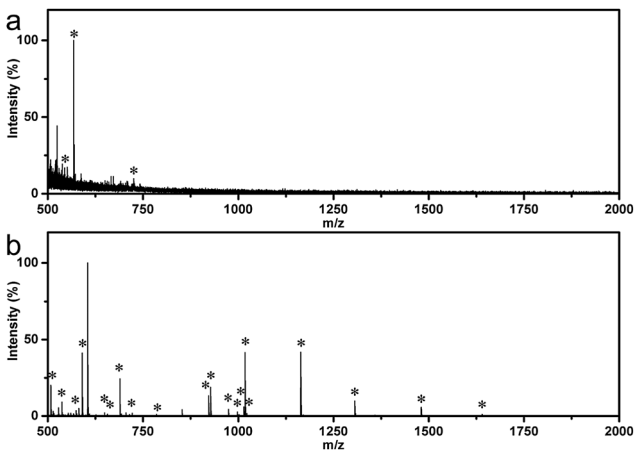

Fig. 7 MALDI-TOF mass spectra of the diluted digest of BSA (5 fmol μL^{-1}) without any treatment (a), and after enrichment with rGO–Fe_3O_4 composites (b).

weight peptides should be responsible for the adsorption of the low molecular weight peptides.

Conclusion

In conclusion, the GO–Fe_3O_4 and the rGO–Fe_3O_4 composites with good water dispersibility, high affinity and rapid magnetic response have been prepared. Significantly, the GO–Fe_3O_4 composites with hydrophilic groups can be used as an effective absorbent or carriers for rapid separation and immobilization of proteins, while the water dispersible rGO–Fe_3O_4 composites can be used for enrichment of peptides by virtue of their high surface area and special structure. Furthermore, the synthetic route can also be expanded to graphene oxide or graphene systems with other nanostructures. The GO/rGO–Fe_3O_4 composites could also be applied as a carrier for enzyme immobilization for specific functions, capture of biomolecules for water purification, and enrichment of small biomolecules for biomedical applications.

Acknowledgements

This work was supported by the National Natural Science Foundation of China (NNSFC) (Grant no. 20871083 and 21171161).

Notes and references

1 H. Wang, Q. Zhang, X. Chu, T. Chen, J. Ge and R. Yu, *Angew. Chem., Int. Ed.*, 2011, **50**, 7065–7069.
2 S. Stankovich, D. A. Dikin, G. H. Dommett, K. M. Kohlhaas, E. J. Zimney, E. A. Stach, R. D. Piner, S. T. Nguyen and R. S. Ruoff, *Nature*, 2006, **442**, 282–286.
3 V. C. Tung, M. J. Allen, Y. Yang and R. B. Kaner, *Nat. Nanotechnol.*, 2009, **4**, 25–29.
4 R. S. Ruoff, *J. Mater. Chem.*, 2011, **21**, 3272.
5 H.-J. Song, X.-H. Jia, N. Li, X.-F. Yang and H. Tang, *J. Mater. Chem.*, 2012, **22**, 895–902.
6 V. Chandra, J. Park, Y. Chun, J. W. Lee, I.-C. Hwang and K. S. Kim, *ACS Nano*, 2010, **4**, 3979–3986.
7 S. Myung, A. Solanki, C. Kim, J. Park, K. S. Kim and K.-B. Lee, *Adv. Mater.*, 2011, **23**, 2221–2225.
8 S. Guo and S. Dong, *J. Mater. Chem.*, 2011, **21**, 18503–18516.
9 W. Shi, J. Zhu, D. H. Sim, Y. Y. Tay, Z. Lu, X. Zhang, Y. Sharma, M. Srinivasan, H. Zhang, H. H. Hng and Q. Yan, *J. Mater. Chem.*, 2011, **21**, 3422–3427.
10 Y. Lin, Y. Tao, F. Pu, J. Ren and X. Qu, *Adv. Funct. Mater.*, 2011, **21**, 4565–4572.
11 L. Feng, L. Wu, J. Wang, J. Ren, D. Miyoshi, N. Sugimoto and X. Qu, *Adv. Mater.*, 2012, **24**, 125–131.
12 B. Nam, H.-J. Lee, H. Goh, Y. B. Lee and W. S. Choi, *J. Mater. Chem.*, 2012, **22**, 3148–3153.
13 Y. Zhang, J. Zhang, X. Huang, X. Zhou, H. Wu and S. Guo, *Small*, 2012, **8**, 154–159.
14 L. A. L. Tang, J. Wang and K. P. Loh, *J. Am. Chem. Soc.*, 2010, **132**, 10976–10977.
15 B. Gulbakan, E. Yasun, M. I. Shukoor, Z. Zhu, M. You, X. Tan, H. Sanchez, D. H. Powell, H. Dai and W. Tan, *J. Am. Chem. Soc.*, 2010, **132**, 17408–17410.
16 Y. Deng, D. Qi, C. Deng, X. Zhang and D. Zhao, *J. Am. Chem. Soc.*, 2008, **130**, 28–29.
17 H. Chen, C. Deng and X. Zhang, *Angew. Chem.*, 2010, **122**, 617–621.
18 Y. Li, C. Dong, J. Chu, J. Qi and X. Li, *Nanoscale*, 2011, **3**, 280–287.
19 G. Cheng, J. L. Zhang, Y. L. Liu, D. H. Sun and J. Z. Ni, *Chem. Commun.*, 2011, **47**, 5732–5734.
20 B. Li, H. Cao, J. Shao and M. Qu, *Chem. Commun.*, 2011, **47**, 10374–10376.
21 B. Li, H. Cao, J. Shao, M. Qu and J. H. Warner, *J. Mater. Chem.*, 2011, **21**, 5069–5075.
22 C. Deng, J. Meng and C. Shi, *Chem. Commun.*, 2012, **48**, 2418–2420.
23 X. Li, X. Huang, D. Liu, X. Wang, S. Song, L. Zhou and H. Zhang, *J. Phys. Chem. C*, 2011, **115**, 21567–21573.
24 H. He and C. Gao, *ACS Appl. Mater. Interfaces*, 2010, **2**, 3201–3210.
25 X. Yang, X. Zhang, Y. Ma, Y. Huang, Y. Wang and Y. Chen, *J. Mater. Chem.*, 2009, **19**, 2710–2714.
26 H. Sun, L. Cao and L. Lu, *Nano Res.*, 2011, **4**, 550–562.
27 X. Huang, X. Qi, F. Boey and H. Zhang, *Chem. Soc. Rev.*, 2012, **41**, 666–686.
28 W. S. Hummers and R. E. Offeman, *J. Am. Chem. Soc.*, 1958, **80**, 1339.
29 D. C. Marcano, D. V. Kosynkin, J. M. Berlin, A. Sinitskii, Z. Sun, A. Slesarev, L. B. Alemany, W. Lu and J. M. Tour, *ACS Nano*, 2010, **4**, 4806–4814.
30 P. Lu, J.-L. Zhang, Y.-L. Liu, D.-H. Sun, G.-X. Liu, G.-Y. Hong and J.-Z. Ni, *Talanta*, 2010, **82**, 450–457.
31 X. Fan, W. Peng, Y. Li, X. Li, S. Wang, G. Zhang and F. Zhang, *Adv. Mater.*, 2008, **20**, 4490–4493.
32 Z. Lei, L. Lu and X. S. Zhao, *Energy Environ. Sci.*, 2012, **5**, 6391–6399.
33 Y. Liang, D. Wu, X. Feng and K. Müllen, *Adv. Mater.*, 2009, **21**, 1679–1683.
34 S. Villar-Rodil, J. I. Paredes, A. Martinez-Alonso and J. M. D. Tascon, *J. Mater. Chem.*, 2009, **19**, 3591–3593.
35 B.-S. Kong, J. Geng and H.-T. Jung, *Chem. Commun.*, 2009, 2174–2176.
36 B. Lukose, A. Kuc and T. Heine, *Chem.–Eur. J.*, 2011, **17**, 2388–2392.
37 G. Xie, P. Xi, H. Liu, F. Chen, L. Huang, Y. Shi, F. Hou, Z. Zeng, C. Shao and J. Wang, *J. Mater. Chem.*, 2012, **22**, 1033–1039.
38 K. Zhou, Y. Zhu, X. Yang and C. Li, *New J. Chem.*, 2010, **34**, 2950–2955.
39 S. Y. Lee, S. Lee, I. H. Kho, J. H. Lee, J. H. Kim and J. H. Chang, *Chem. Commun.*, 2011, **47**, 9989–9991.
40 J. Lee, H. B. Na, B. C. Kim, J. H. Lee, B. Lee, J. H. Kwak, Y. Hwang, J.-G. Park, M. B. Gu, J. Kim, J. Joo, C.-H. Shin, J. W. Grate, T. Hyeon and J. Kim, *J. Mater. Chem.*, 2009, **19**, 7864–7870.
41 M. Zhang, X. He, L. Chen and Y. Zhang, *Nanotechnology*, 2011, **22**, 065705.
42 D. R. Dreyer, S. Park, C. W. Bielawski and R. S. Ruoff, *Chem. Soc. Rev.*, 2010, **39**, 228–240.
43 S. Park, J. An, R. D. Piner, I. Jung, D. Yang, A. Velamakanni, S. T. Nguyen and R. S. Ruoff, *Chem. Mater.*, 2008, **20**, 6592–6594.
44 H.-P. Cong, J.-J. He, Y. Lu and S.-H. Yu, *Small*, 2010, **6**, 169–173.
45 M. Swami, *Nat. Rev. Cancer*, 2010, **10**, 597.

